

Complementarity-Supervised Spectral-Band Routing for Multimodal Emotion Recognition

Zhexian Huang^{1,2,*} Bo Zhao^{1,2,*} Hui Ma^{1,†} Zhishu Liu^{1,3} Jie Zhang¹
Ruixin Zhang⁴ Shouhong Ding⁴ Zitong Yu^{1,†}

¹Great Bay University ²The Chinese University of Hong Kong, Shenzhen

³City University of Hong Kong (Dongguan) ⁴Tencent Youtu Lab
225040199@link.cuhk.edu.cn yuzitong@gbu.edu.cn

*Equal contribution †Corresponding authors

Abstract

Multimodal emotion recognition fuses cues such as text, video, and audio to understand individual emotional states. Prior methods face two main limitations: mechanically relying on independent unimodal performance, thereby missing genuine complementary contributions, and coarse-grained fusion conflicting with the fine-grained representations required by emotion tasks. As inconsistent information density across heterogeneous modalities hinders inter-modal feature mining, we propose the Complementarity-Supervised Multi-Band Expert Network, named *Atsuko*, to model fine-grained complementary features via multi-scale band decomposition and expert collaboration. Specifically, we orthogonally decompose each modality’s features into high, mid, and low-frequency components. Building upon this band-level routing, we design a modality-level router with a dual-path mechanism for fine-grained cross-band selection and cross-modal fusion. To mitigate shortcut learning from dominant modalities, we propose the Marginal Complementarity Module (MCM) to quantify performance loss when removing each modality via bi-modal comparison. The resulting complementarity distribution provides soft supervision, guiding the router to focus on modalities contributing unique information gains. Extensive experiments show our method achieves superior performance on the CMU-MOSI, CMU-MOSEI, CH-SIMS, CH-SIMsv2, and MIntRec benchmarks. Our code is publicly available at: <https://github.com/EddyCodex/Atsuko>

1 Introduction

Emotion is closely related to human cognition, decision-making, and behavior, playing a crucial role in daily life [1]. Since human behavior conveys emotions in various forms, multimodal emotion recognition aims to predict human emotions by leveraging multiple modalities, including visual, acoustic, and linguistic information. Compared to unimodal methods, distinct modalities typically offer complementary, non-redundant information [2–4], enhancing affective behavior prediction and aligning more closely with natural human emotional expression.

In principle, linguistic content, facial expressions, and acoustic prosody provide complementary cues to jointly distinguish subtle emotional states. However, in real-world segments, modality informativeness and reliability vary across samples. Fixed fusion paradigms fail to capture sample-dependent modality importance, potentially biasing learning toward dominant modalities [2, 3]. Furthermore, many fusion frameworks overemphasize cross-modal invariants, inadvertently suppressing modality-specific cues and losing specificity [5]. These issues are especially pronounced in MER, where individuals display inconsistent cross-modal expressions and cue availability varies drastically across segments.

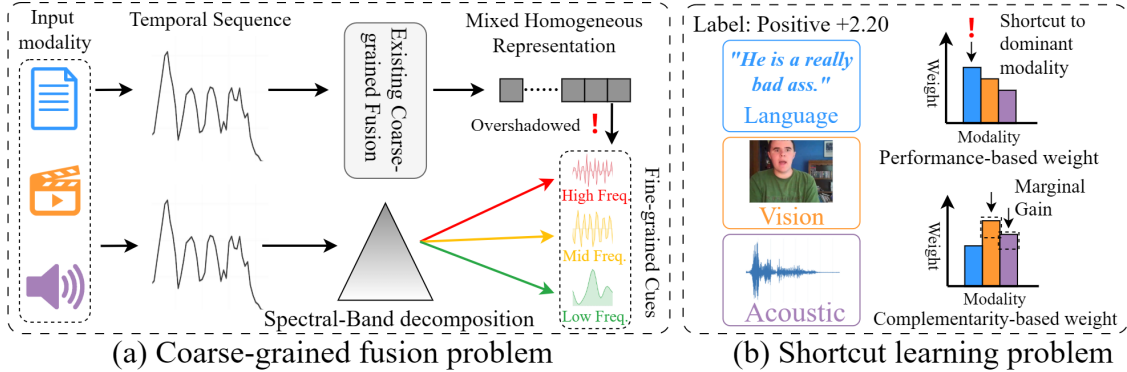


Figure 1: Two fundamental limitations of existing MER methods. (a) Coarse-grained fusion: treating each modality’s temporal features as a homogeneous signal discards fine-grained emotional cues in specific frequency bands. (b) Shortcut learning: performance-based weighting over-relies on the dominant (text) modality, whereas visual and acoustic modalities carry the genuinely complementary cues. Complementarity-based weighting correctly amplifies these contributions.

Substantial research has advanced across cross-modal fusion, modality disentanglement, and dynamic modal balancing. Traditional paradigms evolved from early and late fusion to modeling high-order interactions [6, 7] and unaligned cross-modal attention architectures [8–10]. Despite enhancing interactions, these methods impose uniform fusion rules across samples, ignoring the strong sample-level heterogeneity of emotional expressions. Parallel disentanglement approaches separate shared invariant from private specific subspaces [11] or perform heterogeneous cross-modal distillation [2] to preserve modality-specific cues, generally lacking direct constraints on individual contributions at the final decision stage. Recent balancing strategies [3, 10, 12, 13] mitigate excessive reliance on dominant modalities. However, deriving learning signals from unimodal separability, training dynamics, or heuristic proxy metrics inaccurately reflects the genuine marginal, non-redundant information gain each modality contributes to the multimodal system. As illustrated in Figure 1(b), a modality with strong individual performance may contribute limited incremental information when integrated, whereas a seemingly weaker modality can provide critical complementary cues that significantly enhance multimodal prediction [14, 15].

Beyond modality-level heterogeneity, MER signals exhibit structured intra-modal variability [2, 3, 16]. Emotional cues concentrate at distinct temporal scales, including subtle high-frequency facial micro-movements and prosodic fluctuations [17–20], and are susceptible to selective corruption by noise such as motion blur, occlusions, and background audio [21–23]. Consequently, spectral analysis naturally characterizes these multiscale cues. While widely utilized in speech emotion recognition to isolate emotion-relevant frequencies [18, 19, 24] and recently highlighted for preserving valuable high-frequency components [16], its application to multimodal sequences remains largely unexplored. As Figure 1(a) illustrates, existing fusion frameworks persist in coarse-grained modality-level designs, typically treating temporal features as homogeneous signals and neglecting that distinct frequency components carry varying emotional information.

To address these challenges, we propose the Complementarity-Supervised Multi-Band Expert Network, named Atsuko, to extract fine-grained complementary features via spectral decomposition and expert collaboration. First, to overcome inconsistent information density and selectively attend to emotionally relevant frequencies, we introduce a spectral-band hierarchical routing mechanism. It orthogonally decomposes temporal signals into distinct frequency bands via graph Laplacian eigenvectors and applies a data-driven equal-energy criterion. A lightweight band router then dynamically weights these components based on sample characteristics. Subsequently, a modality-level router with a dual-path decision mechanism recombines these band-filtered features for cross-modal fusion, achieving granular control from spectral details to global representations. Second, to mitigate shortcut learning from dominant modalities, we propose the Marginal

Complementarity Module (MCM) inspired by the Shapley value. By evaluating bimodal scenarios where individual modalities are absent, MCM quantifies each modality’s marginal performance contribution relative to the full trimodal prediction. The resulting complementarity distribution provides soft supervision via Kullback-Leibler divergence minimization to guide the modality router, ensuring the fusion prioritizes modalities supplying unique information gains over redundant independent performance.

The main contributions of this paper are summarized as follows:

- We propose the Spectral-Band Hierarchical Routing Network, which uses a lightweight router to dynamically weight frequency bands based on the signal-to-noise ratio and incorporates a random masking mechanism, effectively enhancing the capability of the model to capture fine-grained high-frequency cues and its robustness against noise interference.
- We design a modality-level router equipped with a dual-path decision mechanism that supports flexible switching between shallow feature spaces and deep semantic decision spaces, thereby achieving granular and interpretable control over the multimodal signal selection process.
- We introduce the Marginal Complementarity Module (MCM), employing complementarity distribution as a soft supervision signal to guide routing learning. This ensures the model focuses on modalities yielding unique information gains, thereby avoiding shortcut learning.

2 Related Works

2.1 Multimodal Emotion Recognition

Multimodal Emotion Recognition (MER) integrates linguistic, visual, and acoustic cues to comprehend human emotions. As a pivotal artificial intelligence domain, MER underpins diverse applications, including driver emotion monitoring [25], mental health screening [26], and online education [27]. Early methods focus on feature fusion via tensors [6, 7] or crossmodal attention [8, 9]. However, these methods typically assume consistent modal contributions across samples, neglecting real-world modal heterogeneity and imbalance. To address this, optimization methods modulate gradient updates [12] or penalize reliance on dominant modalities [28]. Yet, such global adjustments struggle to capture sample level dynamics. Recently, Shapley value approaches [29, 30] have quantified marginal modal contributions for post hoc interpretability. Unlike these primarily post-hoc explanation approaches, our proposed MCM embeds the Shapley value principle directly into training to guide routing, prioritizing modalities that offer genuine complementary information gains. Mixture of Experts (MoE) architectures have extended from unimodal tasks [31–33] to Large Multimodal Models [34, 35]. In affective computing, EMOE [5] pioneers dynamic routing via modality experts to address sample dependencies. Furthermore, hierarchical MoE frameworks [36] enhance robustness against modality missingness, while sparse MoE with interactive distillation [37] utilizes unimodal teachers to mitigate learning ambiguity. Although improving routing flexibility, these decisions predominantly rely on representation strength or similarity, failing to explicitly model complementary contributions. This risks excessive reliance on superficially dominant modalities. Our MCM rectifies this by quantifying the marginal contribution of each modality, explicitly discovering and exploiting multimodal complementary synergies.

2.2 Hierarchical Temporal-Spectral Representation Learning

Emotional cues within temporal signals inherently exhibit multiscale characteristics, where high-frequency components encode transient micro-expressions and low-frequency components convey stable emotional baselines [16, 18]. Early methods leverage wavelets or Fourier spectra to extract energy from fixed bands [19, 24], but static filtering fails to adapt to sample-specific signal-to-noise ratio fluctuations. Although

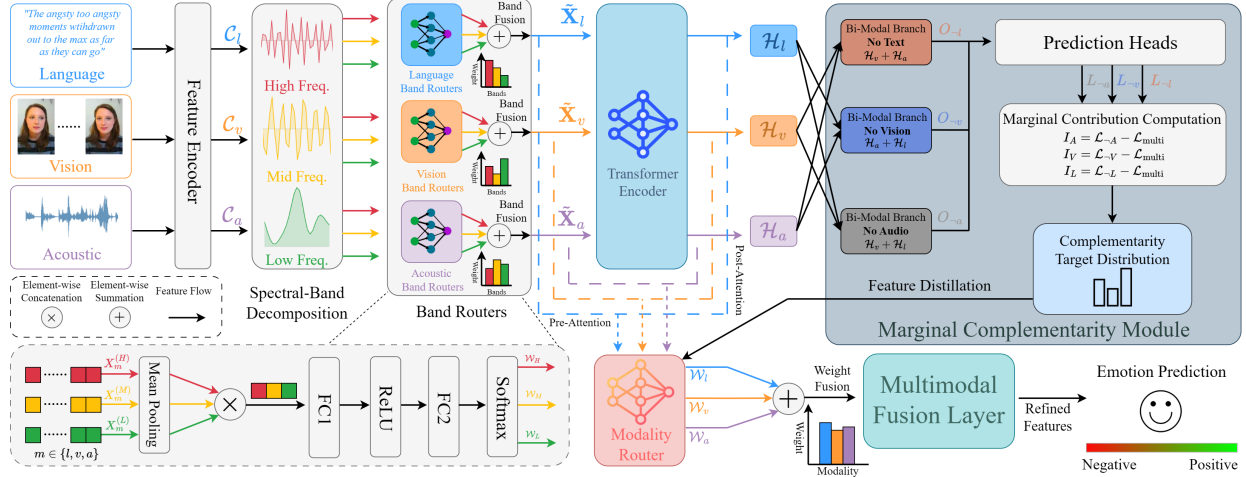


Figure 2: The overall architecture of Atsuko. (1) **Spectral-Band Routing:** Multi-modal temporal inputs are orthogonally decomposed into distinct frequency bands via graph Laplacian and dynamically weighted to yield band-enhanced features \tilde{X}_m . (2) **Modality-Level Routing:** A dual-path mechanism (pre- and post-attention) assigns dynamic fusion weights w_m to the deep semantic features. (3) **Marginal Complementary Module (MCM):** Bimodal contrastive branches quantify each modality’s marginal contribution, providing soft supervision to guide the modality router toward complementary information gains, augmented by feature distillation.

global Fourier mixing [38, 39] reduces attention complexity, its implicit modeling lacks interpretable band separation. Recently, Graph Signal Processing (GSP) provides a principled framework for multimodal temporal analysis. Zhang et al. [40] apply graph Fourier operators to decouple low-frequency consistent semantics from high-frequency complementary ones. Meanwhile, Chen et al. [16] employ message passing on multi-frequency graphs to capture long-range dependencies and fine-grained temporal structures. In parallel, FusionMamba [41] integrates dynamic convolution with state-space models for efficient cross-modal feature enhancement. Additionally, AdaGNN [42] and NFGNN [43] utilize learnable cross-layer and node-level filters to enhance spectral expressiveness. Despite these advancements, existing frequency-domain techniques largely rely on rigid configurations such as equidistant partitioning. This inflexibility exacerbates mismatches caused by divergent cross-modal spectral energy distributions [44–46]. Furthermore, current GSP models primarily learn static filter parameters [47–49]. Applying uniform weights across frequency bands ignores sample-specific variations, often suppressing crucial high-frequency details. Consequently, the dynamic assessment of frequency band reliability tailored to local content remains unexplored in multimodal emotion recognition. To address these gaps, we propose extending dynamic routing to the spectral domain. By utilizing equal-energy partitioning and sample-specific band weighting with random masking, our approach achieves noise-robust, fine-grained control across both frequency and modality levels.

3 The Proposed Method

Figure 2 illustrates the overall architecture of Atsuko. Given linguistic, visual, and acoustic inputs, the model extracts temporal representations via feature encoders and feeds them into the Spectral-Band Hierarchical Routing Network (Section 3.1) for band-level filtering and modality-level aggregation. The Marginal Complementary Module (Section 3.2) then quantifies marginal contributions to guide the routing process toward complementary information gains. Finally, the fused features pass through a prediction layer to yield emotion predictions. The detailed training procedure is summarized in Alg. 1 of the supplementary material.

3.1 Spectral-Band Hierarchical Routing Network

Since emotional cues are distributed across multi-scale frequency components and subject to band-specific noise, we decompose temporal signals into orthogonal spectral bands before adaptive routing. We consider three modalities: linguistic (L), visual (V), and acoustic (A). First, independent one-dimensional temporal convolutional layers are employed for each modality to project raw features into a unified d -dimensional space. Subsequently, a parameter-shared 1×1 convolutional layer is applied to perform cross-modal consistent feature transformation, yielding the temporal representations $X_m \in \mathbb{R}^{T_m \times d}$, where $m \in \{l, v, a\}$.

Unlike FFT, whose fixed sinusoidal bases assume infinite periodicity, ignoring finite-length temporal adjacency, graph Laplacian eigen-decomposition derives orthogonal bases directly from data topology [47, 50]. Thus, we model X_m as a Temporal Path Graph $\mathcal{G} = (\mathcal{V}, \mathcal{E})$, where \mathcal{V} denotes the set of T time steps and \mathcal{E} encompasses all adjacent connections $(t, t + 1)$. Its normalized Laplacian is:

$$\tilde{L} = I - D^{-1/2} A D^{-1/2} \quad (1)$$

where A and D are the adjacency and degree matrices, respectively. Eigen-decomposition yields $\tilde{L} = U \Lambda U^\top$, where $U = [u_1, u_2, \dots, u_T]$ forms the orthogonal eigenvector basis. Smaller eigenvalues λ_k correspond to smoother (low-frequency) basis vectors, while larger ones capture rapid oscillations (high frequencies). We project features into the spectral domain via $\hat{X}_m = U^\top X_m$.

To aggregate the T frequency components into K sub-bands, we must address the long-tail energy distribution: low-frequency components concentrate most energy, whereas high-frequency components, despite low energy, often carry transient emotional cues. Simple equidistant partitioning causes the router to neglect high-frequency bands. We therefore propose an Equal-Energy Partitioning strategy: we compute the cumulative energy distribution CDF(f) by aggregating the average spectral energy density $E_f = \mathbb{E}[\|\hat{X}_m^{(f)}\|_2^2]$ over the training set and determine band boundaries $\mathcal{B} = \{b_0, b_1, \dots, b_K\}$ such that each band contains approximately equal signal energy. Let $U^{(k)} = [u_{b_{k-1}}, \dots, u_{b_k-1}] \in \mathbb{R}^{T \times (b_k - b_{k-1})}$ and $\hat{X}_m^{(k)} \in \mathbb{R}^{(b_k - b_{k-1}) \times d}$ denote the eigenvector sub-matrix and spectral coefficients for the k -th band. The band component is reconstructed via $X_m^{(k)} = U^{(k)} \hat{X}_m^{(k)}$. This decomposition guarantees $\sum_{k=1}^K X_m^{(k)} = X_m$, i.e., orthogonal decoupling with zero information loss. The resulting orthogonality enables the subsequent band routing to independently evaluate and weight each frequency component, preventing the systematic underestimation of high-frequency emotional cues.

To dynamically evaluate the emotional relevance of each band under sample-specific signal-to-noise variations, we design a lightweight Band Router \mathcal{R}_{band} . For each band component $X_m^{(k)}$, average pooling extracts the summary vector $h_m^{(k)} = \text{Pool}(X_m^{(k)}) \in \mathbb{R}^d$. All summaries are concatenated and fed into an MLP to produce dynamic weights, then the enhanced representation is refined:

$$\alpha_m = \text{Softmax} \left(\frac{\text{MLP}([h_m^{(1)} \oplus h_m^{(2)} \oplus \dots \oplus h_m^{(K)}])}{\tau_1} \right), \quad \tilde{X}_m = \sum_{k=1}^K \alpha_{m,k} \cdot X_m^{(k)} \quad (2)$$

where \oplus denotes concatenation and τ_1 is the temperature coefficient.

To further strengthen robustness, we apply Stochastic Band Masking during training: a Bernoulli mask $M \in \{0, 1\}^K$ with probability p is applied to the weights as $\hat{\alpha}_m = (\alpha_m \odot M) / (\sum(\alpha_m \odot M) + \epsilon)$, compelling the router to seek alternative cues when specific bands are absent.

Following intra-modal band enhancement, a modality-level router \mathcal{R}_{modal} dynamically allocates fusion weights across modalities. It is implemented as a two-layer linear network with intermediate L_2 normalization onto a unit hypersphere, ensuring decisions depend on feature directionality rather than magnitude, as heterogeneous modalities inherently produce features at disparate scales:

$$w = \text{Softmax} \left(\frac{W_2 \cdot \text{ReLU}(\hat{z})}{\tau_2} \right), \quad \hat{z} = \frac{W_1 Z_{decision}}{\|W_1 Z_{decision}\|_2} \quad (3)$$

where $W_1 \in \mathbb{R}^{d_h \times d_{in}}$ and $W_2 \in \mathbb{R}^{3 \times d_h}$ are learnable parameters. Two routing pathways are supported:

1. **Pre-Attention Path:** $Z_{decision} = [\text{Pool}(\tilde{X}_l) \oplus \text{Pool}(\tilde{X}_v) \oplus \text{Pool}(\tilde{X}_a)]$, computed before Transformer encoding. This decouples routing from deep feature extraction, preventing encoder output variance from interfering with weight estimation.
2. **Post-Attention Path:** $Z_{decision} = [H_l \oplus H_v \oplus H_a]$, where $H_m = \mathcal{F}_{enc}(\tilde{X}_m)_{[-1]}$ is the final-position output of the Transformer encoder. Self-attention implicitly aggregates the full sequence context, providing a compact semantic summary suitable for subtle emotional expressions requiring contextual reasoning.

The deep semantic representations are then weighted and summed, and then refined via a residual MLP. The prediction head then outputs the emotion prediction.

$$O_{multi} = \sum_m w_m H_m, \quad O'_{multi} = \text{MLP}_{multi}(O_{multi}) + O_{multi} \quad (4)$$

3.2 Marginal Complementarity Module

The fundamental challenge in multimodal fusion lies in ensuring that each modality contributes unique, irreplaceable information rather than redundant common features. A strong modality may exhibit substantial redundancy with others, whereas a seemingly weaker modality can offer critical information gain. To capture this, we propose the Marginal Complementarity Module (MCM), which quantifies the marginal contribution of each modality m by comparing system performance with and without it, rather than relying on standalone unimodal performance. We construct three parallel bimodal branches that simulate scenarios where each modality is absent. For modality m , the bimodal prediction is computed from the remaining deep semantic features $H_{m'}$ ($m' \neq m$), reusing the shared semantic encoders with independent prediction heads:

$$O_{-m} = \mathcal{F}_{-m} \left(\sum_{m' \neq m} H_{m'} \right), \quad m \in \{l, v, a\} \quad (5)$$

where \mathcal{F}_{-m} is a prediction network for the specific bimodal combination. Jointly trained with the full-modal branch to approximate the ground truth y , these branches establish reliable baselines whose performance gap with O_{multi} reflects the excluded modality’s marginal effect. We define Complementarity Importance I_m as the per-sample difference between bimodal and full-modal losses, applying a stop-gradient operation to prevent branch training interference. The raw scores are then normalized into the complementarity target distribution:

$$I_m = \text{StopGradient}(\mathcal{L}_{-m} - \mathcal{L}_{multi}), \quad P_{comp} = \text{Softmax}([I_l, I_v, I_a] / \tau_{comp}) \quad (6)$$

where τ_{comp} controls the distribution sharpness. We inject this complementarity prior into the routing process by minimizing the KL divergence between P_{comp} and the modality routing weights w (Section 3.1):

$$\mathcal{L}_{mcm} = D_{KL}(P_{comp} \parallel w) = \sum_{m \in \{l, v, a\}} P_{comp}[m] \log \left(\frac{P_{comp}[m]}{w_m} \right) \quad (7)$$

This constraint guides the router to prioritize modalities yielding genuine complementary gains, circumventing shortcut learning from dominant modalities. To ensure the fused representation preserves router-identified complementary information, we introduce feature distillation. Each modality’s semantic representation is

refined via an independent residual MLP: $H'_m = \text{MLP}_m(H_m) + H_m$, where MLP_m comprises two linear layers with ReLU activation. The teacher signal is a router-weighted combination of these refined representations:

$$\mathcal{T}_{feat} = \text{StopGradient}\left(\sum_{m \in \{l, v, a\}} w_m H'_m\right) \quad (8)$$

Since \mathcal{L}_{mcm} optimizes w_m , \mathcal{T}_{feat} constitutes a complementarity-aware feature combination where low-weight (noisy) modalities are naturally attenuated. We align fused features with this teacher by minimizing distributional discrepancy:

$$\mathcal{L}_{distill} = \frac{1}{D} \sum_{j=1}^D (\text{Softmax}(O'_{multi})_j - \text{Softmax}(\mathcal{T}_{feat})_j)^2 \quad (9)$$

This forms a closed loop: the MCM identifies complementarity at the decision level via w , while the distillation enforces it at the feature level via $\mathcal{L}_{distill}$.

3.3 Loss Function

The total training objective integrates the task loss, complementarity routing loss, and entropy regularization terms. The task loss aggregates the primary and auxiliary prediction objectives:

$$\mathcal{L}_{task} = \mathcal{L}_{multi} + \mathcal{L}_{uni} + \lambda_{sub} \mathcal{L}_{sub} \quad (10)$$

where \mathcal{L}_{multi} is the full-modal primary loss, $\mathcal{L}_{uni} = \frac{1}{3}(\mathcal{L}_l + \mathcal{L}_v + \mathcal{L}_a)$ is the mean unimodal auxiliary loss, and $\mathcal{L}_{sub} = \frac{1}{3}(\mathcal{L}_{va} + \mathcal{L}_{la} + \mathcal{L}_{lv})$ is the MCM-introduced average bimodal branch loss, weighted by λ_{sub} . To prevent routing collapse to a single modality or band, we apply entropy regularization to both modality (\mathbf{w}) and band (α_m) routing weights. The modality-level form is:

$$\mathcal{L}_{ety} = \frac{N}{B} \sum_{i=1}^B \sum_{m=1}^N w_m^{(i)} \log w_m^{(i)} \quad (11)$$

where N is the number of modalities and B is the batch size. Minimizing \mathcal{L}_{ety} maximizes the entropy of the weight distribution, encouraging balanced modality utilization. The band-level entropy regularization \mathcal{L}_{band} follows the same formulation applied to α_m for each modality. The complementarity routing loss \mathcal{L}_{mcm} and feature distillation loss $\mathcal{L}_{distill}$ are defined in Section 3.2. The final total loss is:

$$\mathcal{L}_{total} = \mathcal{L}_{task} + \lambda_{ety} \mathcal{L}_{ety} + \lambda_{mcm} \mathcal{L}_{mcm} + \lambda_{dist} \mathcal{L}_{distill} + \lambda_{band} \mathcal{L}_{band} \quad (12)$$

where λ_{sub} , λ_{ety} , λ_{mcm} , λ_{dist} , and λ_{band} are hyperparameters.

4 Experiments

To evaluate the generality of our proposed method, we conduct experiments on five public datasets covering both Multimodal Emotion Recognition (MER) and Multimodal Intent Recognition (MIR), including CMU-MOSI [51], CMU-MOSEI [52], CH-SIMS [53], CH-SIMSv2 [54], and MIntRec [55]. For emotion datasets we report Acc-7 (MOSI/MOSEI), Acc-5/Acc-3 (CH-SIMS/v2), Acc-2, F1, and MAE; for MIntRec we report Accuracy, F1, Precision, and Recall. Implementation details and per-dataset hyperparameters are provided in the supplementary material.

Methods	Setting	MOSI				MOSEI			
		ACC7 \uparrow	ACC2 \uparrow	F1 \uparrow	MAE \downarrow	ACC7 \uparrow	ACC2 \uparrow	F1 \uparrow	MAE \downarrow
EF-LSTM [6]	Aligned	33.7	75.3	75.2	1.386	47.4	78.2	77.9	0.620
LF-DNN [6]		31.5	78.4	78.3	0.972	51.7	83.5	83.1	0.568
TFN [6]		31.9	78.8	78.9	0.953	50.9	80.4	80.7	0.574
LMF [7]		36.9	78.7	78.7	0.931	52.3	84.7	84.5	0.564
MFN [9]		35.6	78.4	78.4	0.964	50.8	84.0	84.0	0.574
Graph-MFN [52]		31.5	78.1	78.1	0.970	51.6	84.6	84.5	0.553
MulT [8]		35.1	80.0	80.1	0.936	52.3	82.7	82.8	0.572
MISA [11]		41.8	84.2	84.2	0.754	52.3	85.3	85.1	0.543
Self-MM [56]		45.3	84.9	84.9	0.738	53.2	84.5	84.3	0.540
MMIM [57]		45.8	84.6	84.5	0.717	50.1	83.6	83.5	0.580
DMD [58]		46.2	83.2	83.2	0.721	52.4	84.8	84.7	0.546
EMOE [5]		47.7	85.4	85.4	0.710	54.1	85.3	85.3	0.536
Atsuko(Ours)		48.7	86.3	86.2	0.696	54.4	85.6	85.7	0.530
EF-LSTM [6]	Unaligned	31.0	73.6	74.5	1.420	46.3	76.1	75.9	0.594
LF-DNN [6]		32.5	78.2	78.3	0.987	52.3	83.7	83.2	0.561
TFN [6]		35.3	76.5	76.6	0.995	50.2	84.2	84.0	0.573
LMF [7]		31.1	79.1	79.1	0.963	51.9	83.8	83.9	0.565
MFN [9]		34.7	80.0	80.1	0.971	51.3	83.2	83.3	0.567
Graph-MFN [52]		34.4	79.4	79.2	0.930	51.8	84.2	84.2	0.568
MulT [8]		33.2	80.3	80.3	0.933	53.2	84.0	84.0	0.556
MISA [11]		43.6	83.8	83.9	0.742	51.0	84.8	84.8	0.557
Self-MM [56]		45.7	83.4	83.6	0.724	52.9	85.3	84.8	0.535
MMIM [57]		45.9	83.4	83.4	0.777	52.6	81.5	81.3	0.578
DMD [58]		46.7	84.0	84.0	0.721	53.1	84.7	84.7	0.536
EMOE [5]		47.8	85.4	85.3	0.697	53.9	85.5	85.5	0.530
Atsuko(Ours)		49.4	86.0	85.9	0.691	54.5	85.7	85.6	0.530

Table 1: Performance comparison on CMU-MOSI and CMU-MOSEI datasets under aligned and unaligned settings. The best results are highlighted in **bold**. \uparrow indicates higher is better; \downarrow indicates lower is better.

4.1 Comparison with the State-Of-The-Art Methods

4.1.1 Results on the English MER Datasets.

As shown in Table 1, Atsuko consistently achieves the best results on both CMU-MOSI and CMU-MOSEI under aligned and unaligned settings. On CMU-MOSI, the advantage is most pronounced in the unaligned setting, where Acc-7 reaches 49.4%, surpassing EMOE by 1.6 percentage points with an MAE of 0.691. Under the aligned setting, Acc-7 improves by 1.0 point and MAE decreases by 0.014 relative to EMOE. These gains on a dataset characterized by limited samples and complex emotional expressions confirm the effectiveness of our method in fine-grained emotion discrimination. On the larger CMU-MOSEI, Atsuko uniformly surpasses all baselines under both settings, with the unaligned Acc-7 reaching 54.5% and MAE attaining 0.530. Given that MOSEI features inconsistent modality quality and significant inter-sample variance, these results indicate the model effectively identifies valuable per-sample modality contributions, thereby reducing prediction errors in emotion regression.

4.1.2 Results on the Chinese MER Datasets.

As shown in Table 2, Atsuko achieves the best results on both Chinese datasets. On CH-SIMS, the model surpasses all baselines across every metric, with Acc-5 improving by 2.19 percentage points over the second-best method EMOE, confirming its capability in processing Chinese multimodal emotional semantics. On the larger CH-SIMSv2, Atsuko attains the highest Acc-5, Acc-2, F1, and average scores despite slightly trailing BBFN on Acc-3, with the overall average improving by 0.55 percentage points over EMOE. These consistent results validate the cross-lingual generalization and stability of the proposed method in large-scale scenarios.

Methods	SIMS					SIMS_v2				
	ACC5 ↑	ACC3 ↑	ACC2 ↑	F1 ↑	Avg ↑	ACC5 ↑	ACC3 ↑	ACC2 ↑	F1 ↑	Avg ↑
TFN [6]	39.30	65.12	78.38	78.62	65.36	52.55	72.21	80.14	80.14	71.26
LMF [7]	40.53	64.68	77.77	77.88	65.19	47.79	64.90	74.18	73.88	65.19
Self-MM [56]	41.53	65.47	80.04	80.44	66.87	52.77	72.61	79.69	76.76	70.46
BBFN [59]	40.92	61.05	78.12	77.88	64.49	53.29	74.47	78.53	78.41	71.18
CENet [60]	33.92	62.58	77.90	77.53	63.66	53.04	73.1	79.56	79.63	71.33
EMOE [5]	42.23	65.43	79.64	79.69	66.75	53.71	71.08	80.85	80.76	71.60
Atsuko(Ours)	44.42	66.74	80.41	80.21	67.95	54.16	72.15	81.17	81.12	72.15

Table 2: Performance comparison on CH-SIMS and CH-SIMS_v2 datasets. The best results are highlighted in bold.

4.1.3 Results on the MIR Dataset.

To validate cross-task generality, we evaluate Atsuko on the multimodal intent recognition dataset MIntRec. As shown in Table 3, Atsuko achieves the highest accuracy (74.16%) and F1 score (71.22%), surpassing all baselines. Compared to EMOE, Atsuko improves precision from 72.08% to

Methods	ACC ↑	F1 ↑	P ↑	R ↑
MAG-BERT [61]	70.34	68.19	68.31	69.36
MuT [8]	72.58	69.36	70.73	69.47
MISA [11]	72.36	70.57	71.24	70.41
EMOE [5]	72.58	70.73	72.08	70.86
Atsuko (Ours)	74.16	71.22	72.93	70.86

Table 3: Results on MIntRec dataset.

72.93% while matching its recall, indicating that complementarity modeling sharpens the decision boundary. Since MIntRec comprises 20 fine-grained intent categories with an imbalanced distribution, these results confirm that routing captures discriminative cues in long-tail categories and generalizes effectively beyond emotion recognition.

4.2 Ablation Study

To further validate the effectiveness of the proposed method, we conduct comprehensive ablation studies on the MOSI and MOSEI datasets.

SBN	MCM	MOSI				MOSEI			
		ACC7 ↑	ACC2 ↑	F1 ↑	MAE ↓	ACC7 ↑	ACC2 ↑	F1 ↑	MAE ↓
		46.0	83.5	83.5	0.716	52.3	83.8	83.7	0.558
✓		47.1	85.5	85.5	0.701	53.0	85.1	85.2	0.548
	✓	46.9	85.4	85.3	0.700	53.8	85.2	85.1	0.535
✓	✓	48.7	86.3	86.2	0.696	54.4	85.6	85.7	0.530

Table 4: Ablation study of the key components in Atsuko on MOSI and MOSEI dataset. ↑ indicates higher is better; ↓ indicates lower is better.

4.2.1 Quantitative Analysis.

Table 4 presents the ablation results on the MOSI and MOSEI datasets. Each proposed module independently improves overall performance, with complementary contributions. The SBN primarily benefits classification metrics: on MOSI, Acc-2 and F1 rise by approximately 2.0 percentage points, while on MOSEI, Acc-2 gains 1.3 points. By decomposing temporal signals into orthogonal frequency bands and applying dynamic weighting, the SBN effectively isolates fine-grained emotional cues distributed across different frequencies. In contrast, the MCM yields larger gains on regression-oriented metrics. On MOSEI, the MCM alone reduces MAE by 0.023, surpassing the SBN-only reduction of 0.010, confirming that explicitly quantifying the marginal contribution of each modality suppresses redundant information and improves intensity-level prediction. Combining both modules, the full Atsuko model achieves the best results across all metrics, indicating a synergistic effect: the SBN supplies high-quality band-decoupled representations at the feature level, while the MCM ensures they are fused according to genuine information gain at the decision level. A detailed modality contribution analysis under different bimodal and trimodal combinations is provided in the supplementary material.

4.2.2 Sensitivity Analysis.

We sweep four key hyperparameters over broad ranges while fixing the others at their defaults: the entropy regularization weight λ_{ety} , the stochastic mask rate p , the complementarity routing loss weight λ_{mcm} , and the feature distillation loss weight λ_{dist} . Figure 3 reports Acc-7 (%) on CMU-MOSI and CMU-MOSEI. For λ_{ety} (Figure 3(a)), Acc-7 varies by only 1.51 points on MOSI and 0.60 points on MOSEI across the range [0.1, 1.0], with the default value of 1.0 achieving the best result. For the mask rate p (Figure 3(b)), performance peaks at the default $p=0.15$ and degrades gracefully as p increases; even at $p=0.9$, MOSI Acc-7 drops by only 1.87 points, confirming that the MCM complementarity estimation tolerates substantial masking noise. For λ_{mcm} and λ_{dist} (Figures 3(c)–(d)), both achieve their optima at the default value of 0.1; larger values

over-constrain the router or shift optimization away from the task loss, yet the total variation remains within 1.08 and 1.01 points on MOSI and 1.15 points on MOSEI.

Overall, the maximum Acc-7 variation across all four hyperparameters is bounded within 1.87 points on MOSI and 1.15 points on MOSEI, confirming that the default configuration generalizes well without per-dataset tuning.

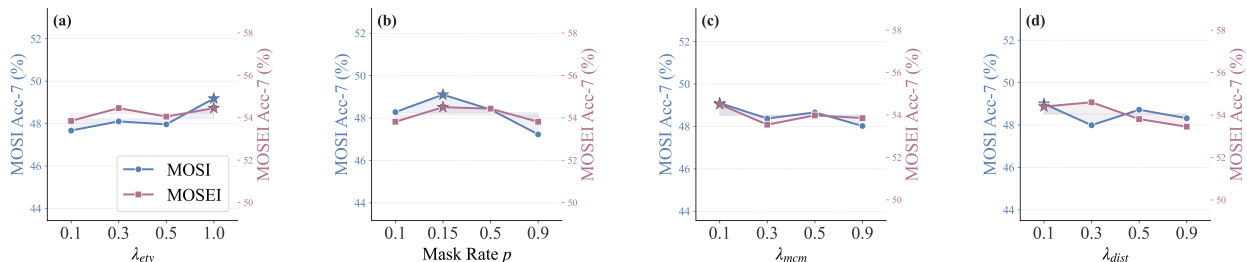


Figure 3: Hyperparameter sensitivity analysis on CMU-MOSI and CMU-MOSEI (Acc-7, %). Each sub-figure sweeps one hyperparameter while holding all others at their default values. The star marker (★) denotes the default configuration adopted in all experiments. Blue lines: MOSI (left y-axis); red lines: MOSEI (right y-axis).

4.2.3 Visualization of Feature Distribution.

Figure 4 presents t-SNE visualizations of multimodal features on the MOSI test set under four ablation configurations. The baseline model produces disorganized embeddings with entangled sentiment polarities, confirming that naive concatenation cannot decouple emotional semantics. Introducing either the SBN or the MCM alone yields improved clustering structure, yet inter-class boundaries remain ambiguous. Atsuko model produces the most compact and well-separated clusters, indicating that the SBN filters modality noise while the MCM enhances discriminability via complementarity supervision, and synergy substantially elevates semantic separability.

4.2.4 Visualization of Marginal Complementarity Module.

To examine how the MCM influences routing decisions, we visualize modality weights for 10 randomly selected CMU-MOSI test samples in Figure 5. Two observations emerge. First, for samples where the baseline misclassifies sentiment polarity, the MCM adaptively reallocates weights toward non-dominant modalities, leveraging prosodic and facial cues to correct predictions. This confirms that the MCM suppresses shortcut reliance on a single modality when other modalities carry genuinely complementary cues. Second, when the textual modality does provide the largest marginal contribution, the MCM appropriately increases its weight, demonstrating that the mechanism does not uniformly penalize the dominant modality but rather faithfully reflects per-sample complementarity. Together, these results show that the router distributes attention according to marginal contributions rather than feature confidence alone.

4.2.5 Visualization of Spectral Band Decomposition.

To verify whether the SBN captures fine-grained emotional cues, we visualize the spectral band decomposition for a strongly positive sample (Label: +2.0) from the CMU-MOSI test set, showing spectral energy distributions, time-domain band decompositions, and learned router weights across all three modalities.

As shown in Figure 6a, Figure 6b, and Figure 6c, the three modalities exhibit distinct spectral structures that the router exploits adaptively. For audio (Figure 6a), the low-frequency band shows flat energy corresponding to background noise with limited emotional discriminability, while the mid- and high-frequency bands capture

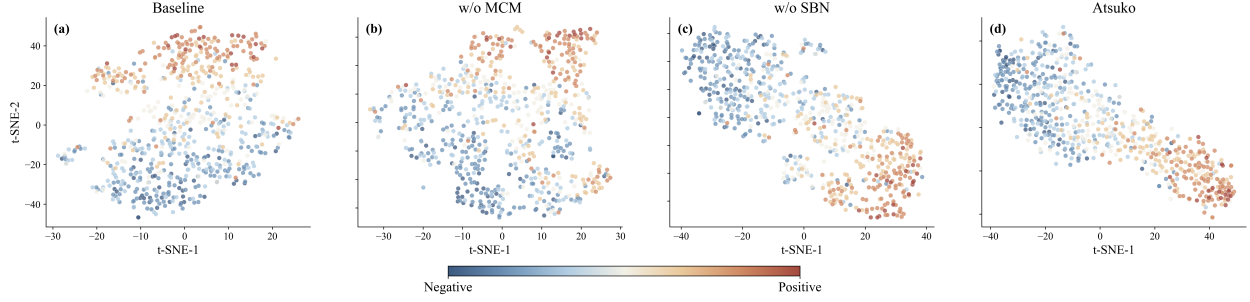


Figure 4: t-SNE visualization of feature distributions on MOSI test set. (a) Baseline (w/o SBN & MCM), (b) w/o MCM, (c) w/o SBN, and (d) Atsuko (Full). Different colors represent varying sentiment intensities. The proposed method shows clearer cluster margins and better separability.

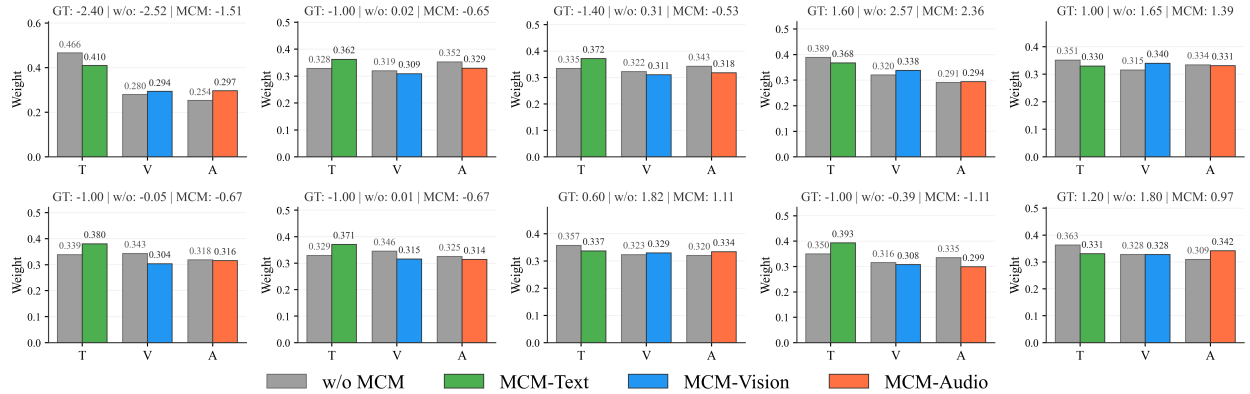
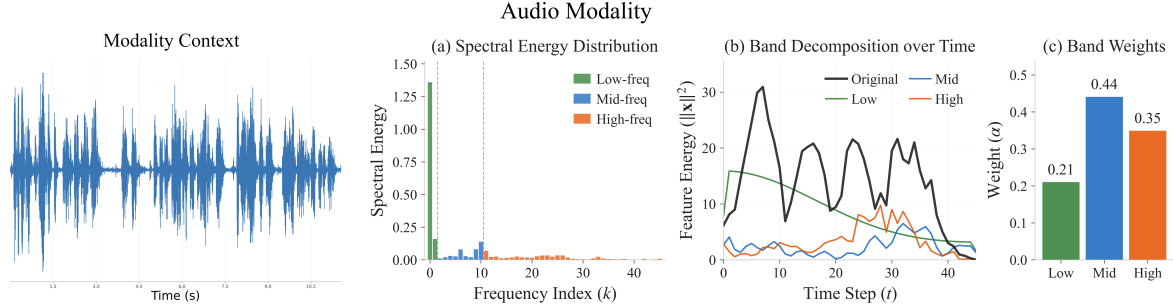
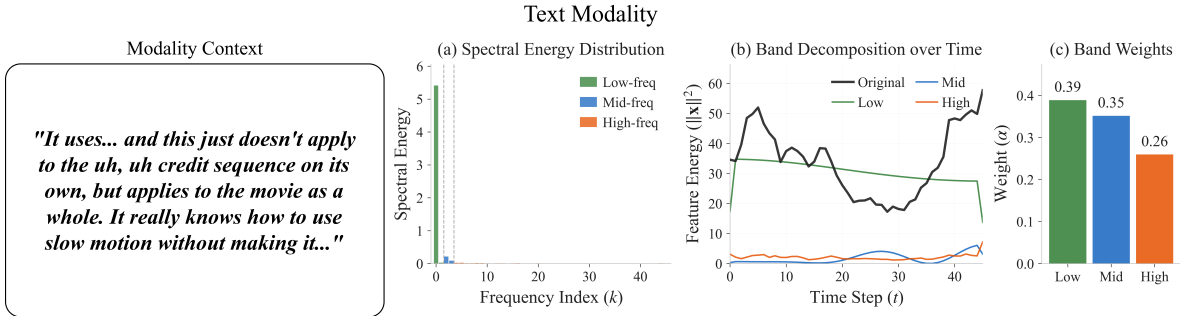


Figure 5: Visualization of modality weights predicted by the router on randomly selected CMU-MOSI test samples. Gray bars denote the baseline model without MCM, and colored bars denote the MCM-enhanced model.

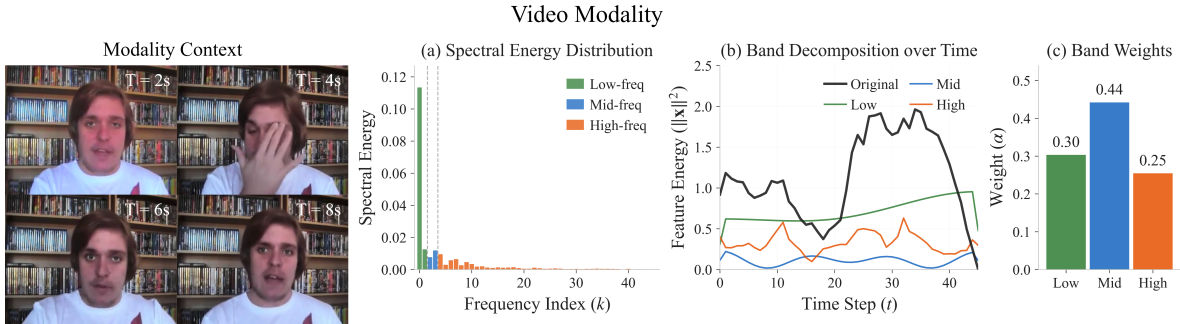
prosodic fluctuations and transient acoustic events such as stress and pauses. The router accordingly assigns dominant weights to mid ($\alpha_{mid} \approx 0.44$) and high ($\alpha_{high} \approx 0.35$) frequencies, suppressing the uninformative low-frequency components. For text (Figure 6b), energy concentrates in ultra-low frequency bands ($k = 0, 1$), reflecting deep semantic features from BERT that encode global contextual information with smooth temporal evolution. The router assigns dominant weight to the low-frequency band ($\alpha_{low} \approx 0.39$), correctly identifying that core emotional semantics reside in stable contextual representations. For vision (Figure 6c), the low-frequency band encodes static baselines such as identity and head pose, whereas the mid-frequency band captures subtle facial muscle movements and lip dynamics critical for expression recognition. The router assigns the highest weight to the mid-frequency band ($\alpha_{mid} \approx 0.44$), focusing on dynamic facial regions. Across modalities, feature energy follows a clear hierarchy (text > audio > vision), reflecting inherent differences in information density: BERT features encapsulate dense semantic information per time step, acoustic features combine continuity with discrete prosodic variations, and visual features exhibit high inter-frame redundancy. Through spectral band routing, the SBN bridges these order-of-magnitude energy differences to adaptively extract prosodic cues from audio, global semantics from text, and facial dynamics from vision, achieving effective multimodal fusion aligned with human perceptual mechanisms.



(a) **Audio** modality. Each panel shows: (a) spectral energy distribution, where colored regions indicate low/mid/high-frequency bands; (b) time-domain feature energy $\|\mathbf{x}\|^2$ decomposed into three bands; (c) learned routing weights α . The same panel layout applies to (b) and (c) below.



(b) **Text** modality (same sample and panel layout).



(c) **Vision** modality (same sample and panel layout).

Figure 6: Spectral band decomposition of a strongly positive sample (Label: +2.00) from the CMU-MOSI test set across all three modalities.

5 Conclusion

This paper presents Atsuko, a complementarity-supervised multi-band expert network for multimodal emotion recognition that addresses coarse-grained fusion and modality dominance. The Spectral-Band Hierarchical Routing Network extends dynamic routing into the spectral domain, enabling fine-grained decoupling and adaptive selection of emotional cues from heterogeneous signals. The Marginal Complementarity Module incorporates cooperative game theory to explicitly quantify each modality’s marginal contribution, enforcing reliance on genuinely complementary evidence and mitigating shortcut learning. Experiments across five benchmarks validate the superior performance, robustness, and interpretability of our method. The proposed spectral-temporal routing paradigm offers a versatile fusion framework for finer-grained representation decoupling in affective computing.

References

- [1] R. W. Picard. *Affective Computing*. MIT Press, Cambridge, MA, USA, 2000.
- [2] S. Wei, Y. Luo, Y. Wang, and C. Luo. Robust Multimodal Learning via Representation Decoupling. In *Computer Vision – ECCV 2024*, pages 38–54, 2024. doi: 10.1007/978-3-031-72946-1_3.
- [3] Y. Wei, S. Li, R. Feng, and D. Hu. Diagnosing and Re-learning for Balanced Multimodal Learning. In *Computer Vision – ECCV 2024*, pages 71–86, 2024. doi: 10.1007/978-3-031-73039-9_5.
- [4] Q. Ye, Z. Yu, R. Shao, Y. Cui, X. Kang, X. Liu, P. Torr, and X. Cao. CAT+: Investigating and Enhancing Audio-visual Understanding in Large Language Models. *IEEE Transactions on Pattern Analysis and Machine Intelligence*, 47(10), 2025.
- [5] Y. Fang, W. Huang, G. Wan, K. Su, and M. Ye. EMOE: Modality-Specific Enhanced Dynamic Emotion Experts. In *Proceedings of the IEEE/CVF Conference on Computer Vision and Pattern Recognition (CVPR)*, pages 14314–14324, 2025. doi: 10.1109/CVPR52734.2025.01335.
- [6] A. Zadeh, M. Chen, S. Poria, E. Cambria, and L.-P. Morency. Tensor Fusion Network for Multimodal Sentiment Analysis. In *Proceedings of the 2017 Conference on Empirical Methods in Natural Language Processing (EMNLP)*, pages 1103–1114, 2017. doi: 10.18653/v1/D17-1115.
- [7] Z. Liu, Y. Shen, V. B. Lakshminarasimhan, P. P. Liang, A. Zadeh, and L.-P. Morency. Efficient Low-rank Multimodal Fusion with Modality-Specific Factors. *arXiv preprint arXiv:1806.00064*, 2018.
- [8] Y.-H. H. Tsai, S. Bai, P. P. Liang, J. Z. Kolter, L.-P. Morency, and R. Salakhutdinov. Multimodal Transformer for Unaligned Multimodal Language Sequences. In *Proceedings of the 57th Annual Meeting of the Association for Computational Linguistics (ACL)*, pages 6558–6569, 2019. doi: 10.18653/v1/P19-1656.
- [9] A. Zadeh, P. P. Liang, N. Mazumder, S. Poria, E. Cambria, and L.-P. Morency. Memory Fusion Network for Multi-view Sequential Learning. In *Proceedings of the AAAI Conference on Artificial Intelligence (AAAI)*, volume 32, 2018.
- [10] K. Yuan, Z. Yu, X. Liu, W. Xie, H. Yue, and J. Yang. AUFormer: Vision Transformers are Parameter-Efficient Facial Action Unit Detectors. In *Proceedings of the European Conference on Computer Vision (ECCV)*, 2024.
- [11] D. Hazarika, R. Zimmermann, and S. Poria. MISA: Modality-Invariant and -Specific Representations for Multimodal Sentiment Analysis. In *Proceedings of the 28th ACM International Conference on Multimedia (ACM MM)*, pages 1122–1131, 2020. doi: 10.1145/3394171.3413678.
- [12] X. Peng, Y. Wei, A. Deng, D. Wang, and D. Hu. Balanced Multimodal Learning via On-the-fly Gradient Modulation. In *Proceedings of the IEEE/CVF Conference on Computer Vision and Pattern Recognition (CVPR)*, pages 8238–8247, 2022.
- [13] X. Lin, A. Liu, Z. Yu, R. Cai, S. Wang, Y. Yu, J. Wan, Z. Lei, X. Cao, and A. Kot. Reliable and Balanced Transfer Learning for Generalized Multimodal Face Anti-Spoofing. *IEEE Transactions on Pattern Analysis and Machine Intelligence*, 2025.
- [14] C. Peng, K. Chen, L. Shou, and G. Chen. CARAT: Contrastive Feature Reconstruction and Aggregation for Multi-Modal Multi-Label Emotion Recognition. *arXiv preprint arXiv:2312.10201*, 2023.

- [15] X. Zhang, J. Yoon, M. Bansal, and H. Yao. Multimodal Representation Learning by Alternating Unimodal Adaptation. In *Proceedings of the IEEE/CVF Conference on Computer Vision and Pattern Recognit. (CVPR)*, pages 27456–27466, 2024. doi: 10.1109/CVPR52733.2024.02592.
- [16] F. Chen, J. Shao, S. Zhu, and H. T. Shen. Multivariate, Multi-Frequency and Multimodal: Rethinking Graph Neural Networks for Emotion Recognition in Conversation. In *Proceedings of the IEEE/CVF Conference on Computer Vision and Pattern Recognition (CVPR)*, pages 10761–10770, 2023.
- [17] X. Fan, X. Chen, M. Jiang, A. R. Shahid, and H. Yan. SelfME: Self-Guided Modal Enhancement on Micro-Expression Recognition. In *Proceedings of the IEEE/CVF Conference on Computer Vision and Pattern Recognition (CVPR)*, pages 13834–13843, 2023.
- [18] A. Satt, S. Rozenberg, and R. Hoory. Efficient Emotion Recognition from Speech Using Deep Learning on Spectrograms. In *Proc. Interspeech*, pages 1089–1093, 2017. doi: 10.21437/Interspeech.2017-200.
- [19] H. Zou, Y. Si, C. Chen, D. Rajan, and E. S. Chng. Speech Emotion Recognition with Co-Attention Based Multi-Level Acoustic Information. In *Proc. IEEE Int. Conf. Acoust., Speech Signal Process. (ICASSP)*, 2022. doi: 10.1109/ICASSP43922.2022.9747095.
- [20] Z. Liu, K. Yuan, B. Zhao, Y. Xu, and Z. Yu. AU-LLM: Micro-Expression Action Unit Detection via Enhanced LLM-Based Feature Fusion. *arXiv preprint arXiv:2507.21778*, 2025.
- [21] X. Wu, M. Zhai, X. Li, W. Wang, and Y. Gong. NorFace: Improving Facial Expression Analysis by Identity Normalization. In *Computer Vision – ECCV 2024*, pages 427–444, 2024. doi: 10.1007/978-3-031-72673-6_24.
- [22] Y. Liu, H. Sun, G. Chen, Q. Wang, Z. Zhao, X. Lu, and L. Wang. Multi-level knowledge distillation for noise robust speech emotion recognition in noisy conditions. In *Proc. Interspeech*, pages 4538–4542, 2023. doi: 10.21437/Interspeech.2023-607.
- [23] Z. Yu, R. Cai, Y. Cui, X. Liu, Y. Hu, and A. Kot. Rethinking Vision Transformer and Masked Autoencoder in Multimodal Face Anti-Spoofing. *arXiv preprint arXiv:2302.05744*, 2023.
- [24] I. Luengo, E. Navas, and I. Hernáez. Combining Spectral and Prosodic Information for Emotion Recognition in the Interspeech 2009 Emotion Challenge. In *Proc. Interspeech*, pages 332–335, 2009. doi: 10.21437/Interspeech.2009-108.
- [25] G. Xiang, S. Yao, X. Wu, H. Deng, G. Wang, Y. Liu, F. Li, and Y. Peng. Driver multi-task emotion recognition network based on multi-modal facial video analysis. *Pattern Recognition*, 161:111241, 2025. doi: 10.1016/j.patcog.2024.111241.
- [26] F. Ringeval, B. Schuller, M. Valstar, N. Cummins, R. Cowie, L. Tavabi, M. Schmitt, S. Alisamir, S. Amiriparian, E.-M. Messner, S. Song, S. Liu, Z. Zhao, A. Mallol-Ragolta, Z. Ren, M. Soleymani, and M. Pantic. AVEC 2019 Workshop and Challenge: State-of-Mind, Detecting Depression with AI, and Cross-Cultural Affect Recognition. *arXiv preprint arXiv:1907.11510*, 2019.
- [27] Q. El Maazouzi and A. Retbi. Multimodal Detection of Emotional and Cognitive States in E-Learning Through Deep Fusion of Visual and Textual Data with NLP. *Computers*, 14(8):314, 2025. doi: 10.3390/computers14080314.
- [28] S. Yerramilli, J. S. Tamarapalli, J. Francis, and E. Nyberg. Attribution Regularization for Multimodal Paradigms. *arXiv preprint arXiv:2404.02359*, 2024.

- [29] L. Parcalabescu and A. Frank. MM-SHAP: A Performance-agnostic Metric for Measuring Multimodal Contributions in Vision and Language Models & Tasks. In *Findings of the Association for Computational Linguistics: ACL 2023*, pages 2492–2509, 2023. doi: 10.18653/v1/2023.findings-acl.158.
- [30] P. Hu, X. Li, and Y. Zhou. SHAPE: A Unified Approach to Evaluate the Contribution and Cooperation of Individual Modalities. In *Proceedings of the Thirty-First International Joint Conference on Artificial Intelligence (IJCAI)*, pages 3064–3070, 2022. doi: 10.24963/ijcai.2022/425.
- [31] W. Fedus, B. Zoph, and N. Shazeer. Switch Transformers: Scaling to Trillion Parameter Models with Simple and Efficient Sparsity. *Journal of Machine Learning Research*, 23(120):1–39, 2022.
- [32] D. Lepikhin, H. Lee, Y. Xu, D. Chen, O. Firat, Y. Huang, M. Krikun, N. Shazeer, and Z. Chen. GShard: Scaling Giant Models with Conditional Computation and Automatic Sharding. *arXiv preprint arXiv:2006.16668*, 2020.
- [33] C. Riquelme, J. Puigcerver, B. Mustafa, M. Neumann, R. Jenatton, A. Susano Pinto, D. Keysers, and N. Houlsby. Scaling Vision with Sparse Mixture of Experts. In *Advances in Neural Information Processing Systems (NeurIPS)*, volume 34, 2021.
- [34] Y. Li, S. Jiang, B. Hu, L. Wang, W. Zhong, W. Luo, L. Ma, and M. Zhang. Uni-MoE: Scaling Unified Multimodal LLMs with Mixture of Experts. *arXiv preprint arXiv:2405.11273*, 2024.
- [35] J. Wu, X. Hu, Y. Wang, B. Pang, and R. Soricut. Omni-SMoLA: Boosting Generalist Multimodal Models with Soft Mixture of Low-rank Experts. In *Proceedings of the IEEE/CVF Conference on Computer Vision and Pattern Recognition (CVPR)*, pages 14205–14215, 2024.
- [36] Y. Zhu, L. Han, G. Jiang, P. Zhou, and Y. Wang. Hierarchical MoE: Continuous Multimodal Emotion Recognition with Incomplete and Asynchronous Inputs. *arXiv preprint arXiv:2508.02133*, 2025.
- [37] J. Li, R. Yu, H. Huang, and H. Yan. Unimodal-driven Distillation in Multimodal Emotion Recognition with Dynamic Fusion. *arXiv preprint arXiv:2503.23721*, 2025.
- [38] J. Lee-Thorp, J. Ainslie, I. Eckstein, and S. Onta nón. FNet: Mixing Tokens with Fourier Transforms. In *Proceedings of the 2022 Conference of the North American Chapter of the Association for Computational Linguistics: Human Language Technologies (NAACL-HLT)*, pages 4296–4313, 2022. doi: 10.18653/v1/2022.naacl-main.319.
- [39] Y. Rao, W. Zhao, Z. Zhu, J. Lu, and J. Zhou. Global Filter Networks for Image Classification. *arXiv preprint arXiv:2107.00645*, 2021.
- [40] T. Meng, F. Zhang, Y. Shou, W. Ai, N. Yin, and K. Li. Revisiting Multimodal Emotion Recognition in Conversation from the Perspective of Graph Spectrum. *arXiv preprint arXiv:2404.17862*, 2024.
- [41] X. Xie, Y. Cui, T. Tan, X. Zheng, and Z. Yu. FusionMamba: Dynamic Feature Enhancement for Multimodal Image Fusion with Mamba. *arXiv preprint arXiv:2404.09498*, 2024.
- [42] Y. Dong, K. Ding, B. Jalaian, S. Ji, and J. Li. AdaGNN: Graph Neural Networks with Adaptive Frequency Response Filter. *arXiv preprint arXiv:2104.12840*, 2021.
- [43] S. Zheng, Z. Zhu, Z. Liu, Y. Li, and Y. Zhao. Node-oriented Spectral Filtering for Graph Neural Networks. *IEEE Transactions on Pattern Analysis and Machine Intelligence*, 2024. doi: 10.1109/TPAMI.2023.3324937.

- [44] S. Zhou, J. Pan, J. Shi, D. Chen, L. Qu, and J. Yang. Seeing the Unseen: A Frequency Prompt Guided Transformer for Image Restoration. In *Computer Vision – ECCV 2024*, volume 15074, pages 246–264, 2024. doi: 10.1007/978-3-031-72640-8_14.
- [45] L. Chen, L. Gu, D. Zheng, and Y. Fu. Frequency-Adaptive Dilated Convolution for Semantic Segmentation. In *Proceedings of the IEEE/CVF Conference on Computer Vision and Pattern Recognition (CVPR)*, pages 3414–3425, 2024.
- [46] X. Wang, G. Xu, H. Jia, and X. Yang. Selective-Stereo: Adaptive Frequency Information Selection for Stereo Matching. In *Proceedings of the IEEE/CVF Conference on Computer Vision and Pattern Recognition (CVPR)*, pages 19701–19710, 2024.
- [47] M. Defferrard, X. Bresson, and P. Vandergheynst. Convolutional Neural Networks on Graphs with Fast Localized Spectral Filtering. In *Advances in Neural Information Processing Systems (NeurIPS)*, volume 29, 2016.
- [48] M. He, Z. Wei, Z. Huang, and H. Xu. BernNet: Learning Arbitrary Graph Spectral Filters via Bernstein Approximation. In *Advances in Neural Information Processing Systems (NeurIPS)*, volume 34, 2021.
- [49] H. Xu, Y. Yan, D. Wang, Z. Xu, Z. Zeng, T. F. Abdelzaher, J. Han, and H. Tong. SLOG: An Inductive Spectral Graph Neural Network Beyond Polynomial Filter. In *Proceedings of the 41st International Conference on Machine Learning (ICML)*, volume 235, pages 55348–55370, 2024.
- [50] D. I. Shuman, S. K. Narang, P. Frossard, A. Ortega, and P. Vandergheynst. The Emerging Field of Signal Processing on Graphs: Extending High-Dimensional Data Analysis to Networks and Other Irregular Domains. *IEEE Signal Processing Magazine*, 30(3):83–98, 2013. doi: 10.1109/MSP.2012.2235192.
- [51] A. Zadeh, R. Zellers, E. Pincus, and L.-P. Morency. MOSI: Multimodal Corpus of Sentiment Intensity and Subjectivity Analysis in Online Opinion Videos. *arXiv preprint arXiv:1606.06259*, 2016.
- [52] A. B. Zadeh, P. P. Liang, S. Poria, E. Cambria, and L.-P. Morency. Multimodal Language Analysis in the Wild: CMU-MOSEI Dataset and Interpretable Dynamic Fusion Graph. In *Proceedings of the 56th Annual Meeting of the Association for Computational Linguistics (Volume 1: Long Papers)*, pages 2236–2246, 2018. doi: 10.18653/v1/P18-1208.
- [53] W. Yu, H. Xu, F. Meng, Y. Zhu, Y. Ma, J. Wu, J. Zou, and K. Yang. CH-SIMS: A Chinese Multimodal Sentiment Analysis Dataset with Fine-grained Annotation of Modality. In *Proceedings of the 58th Annual Meeting of the Association for Computational Linguistics*, pages 3718–3727, 2020. doi: 10.18653/v1/2020.acl-main.343.
- [54] Y. Liu, Z. Yuan, H. Mao, Z. Liang, W. Yang, Y. Qiu, T. Cheng, X. Li, H. Xu, and K. Gao. Make Acoustic and Visual Cues Matter: CH-SIMS v2.0 Dataset and AV-Mixup Consistent Module. *arXiv preprint arXiv:2209.02604*, 2022.
- [55] H. Zhang, H. Xu, X. Wang, Q. Zhou, S. Zhao, and J. Teng. MIntRec: A New Dataset for Multimodal Intent Recognition. In *Proceedings of the 30th ACM International Conference on Multimedia (ACM MM)*, pages 1688–1697, 2022. doi: 10.1145/3503161.3547906.
- [56] W. Yu, H. Xu, Z. Yuan, and J. Wu. Learning Modality-Specific Representations with Self-Supervised Multi-Task Learning for Multimodal Sentiment Analysis. In *Proceedings of the AAAI Conference on Artificial Intelligence (AAAI)*, volume 35, pages 10790–10797, 2021. doi: 10.1609/aaai.v35i12.17289.

- [57] W. Han, H. Chen, and S. Poria. Improving Multimodal Fusion with Hierarchical Mutual Information Maximization for Multimodal Sentiment Analysis. In *Proceedings of the 2021 Conference on Empirical Methods in Natural Language Processing (EMNLP)*, pages 9180–9192, 2021. doi: 10.18653/v1/2021.emnlp-main.723.
- [58] Y. Li, Y. Wang, and Z. Cui. Decoupled Multimodal Distilling for Emotion Recognition. In *Proceedings of the IEEE/CVF Conference on Computer Vision and Pattern Recognition (CVPR)*, pages 6631–6640, 2023. doi: 10.1109/CVPR52729.2023.00641.
- [59] W. Han, H. Chen, A. F. Gelbukh, A. Zadeh, L.-P. Morency, and S. Poria. Bi-Bimodal Modality Fusion for Correlation-Controlled Multimodal Sentiment Analysis. In *Proceedings of the 2021 International Conference on Multimodal Interaction (ICMI)*, pages 6–15, 2021. doi: 10.1145/3462244.3479919.
- [60] D. Wang, S. Liu, Q. Wang, Y. Tian, L. He, and X. Gao. Cross-modal Enhancement Network for Multimodal Sentiment Analysis. *IEEE Transactions on Multimedia*, 25:4909–4921, 2023. doi: 10.1109/TMM.2022.3183830.
- [61] W. Rahman, M. K. Hasan, S. Lee, A. B. Zadeh, C. Mao, L.-P. Morency, and E. Hoque. Integrating Multimodal Information in Large Pretrained Transformers. In *Proceedings of the 58th Annual Meeting of the Association for Computational Linguistics (ACL)*, pages 2359–2369, 2020. doi: 10.18653/v1/2020.acl-main.214.